William P. Schonberg
Civil & Environmental Engineering Department
University of Alabama in Huntsville
Huntsville, AL 35899

Debris Cloud Material Characterization for Hypervelocity Impacts of Single- and Multimaterial Projectiles on Thin Target Plates

The key to conducting an accurate damage assessment of a target impacted by a high speed projectile is the use of a robust assessment methodology. To accurately determine total target damage, a damage assessment methodology must include the effects of discrete impacts by solid debris cloud fragments as well as impulsive loadings due to molten and vaporous debris cloud material. As a result, the amount of debris cloud material in each of the three states of matter must be known to accurately assess total target damage and break-up due to a high speed impact. This article presents a first-principles based method to calculate: the amount of material in a debris cloud created by a perforating hypervelocity impact that is solid, molten, and vaporous; the debris cloud leading edge, trailing edge, center-of-mass, and expansion velocities; and the angular spread of the debris cloud material. The predictions of this methodology are compared against those of empirically based lethality assessment schemes as well as numerical and empirical results obtained in previous studies of debris cloud formation. © *1995 John Wiley & Sons, Inc.*

INTRODUCTION

The key to conducting an accurate damage assessment of a target impacted by a high speed projectile is the use of a robust assessment methodology. The methodology should incorporate all of the significant response characteristics and damage mechanisms that would result from such an impact. The response of a structural target to a high speed impact can be said to consist of two basic and distinct types of response: local response and global response. For high speed impacts, material damage associated with local response occurs within the first several microseconds and is limited to a volume immediately adjacent to the impact site. Global response can refer to any one of a number of global phenomena that occur over a longer period of time (i.e. on the order of milliseconds), under less intense loads, and over a much larger area of the target.

Received May 17, 1994; Accepted January 6, 1995.

Shock and Vibration, Vol. 2, No. 4, pp. 273–287 (1995)

CCC 1070-9622/95/040273-15

Typical global responses include the denting, buckling, tearing, or catastrophic dismemberment of internal missile components.

In high speed impacts, one or more debris clouds are created during the initial impact on the outer wall of a target. These debris clouds spread out as they move through target voids and eventually impact an inner wall or interior component of the target structure. Depending on the impact velocity and the relative material properties of the projectile and target, these debris clouds can contain solid, melted, and vaporized projectile and target materials. The levels of melt and vaporization within the debris clouds in turn determine the nature of the loads transmitted to various target components.

To accurately determine total target damage, a damage assessment methodology must include the effects of discrete impacts by solid debris cloud fragments as well as impulsive loadings due to molten and vaporous debris cloud material. Discrete or simultaneous impacts by individual fragments can pose a lethal threat to an inner wall or to an interior component of a target, depending on the fragments' speed, density, and trajectory, and on the density and strength of the target inner wall or interior component material. Individually, the molten and/or vaporous fragments in a debris cloud may not do significant damage; however, as a whole, they can produce a significant impulsive loading over a relatively large area inside the target. This in turn can result in further damage to the target at later times.

As a result, the amount of debris cloud material in each of the three states of matter must be known to accurately assess total target damage and break-up due to a high speed impact. This article presents a first-principles based method to calculate:

1. the amount of material in a debris cloud created by a perforating hypervelocity impact that is solid, molten, and vaporous;
2. the debris cloud leading edge, trailing edge, center-of-mass, and expansion velocities; and
3. the angular spread of the debris cloud material.

The method presented can be used for single- and multimaterial solid rod projectiles impacting a flat thin target plate. At this point, no adjustments have been made to account for differences in response due to projectile yaw or impact obliquity. The predictions of this methodology are compared against those of empirically based lethality assessment schemes as well as numerical and empirical results obtained in previous studies of hypervelocity impact debris cloud formation.

SHOCK LOADING AND RELEASE ANALYSIS

Consider the normal impact of a right circular cylindrical projectile on a flat target plate as shown in Figure 1. In this study, the projectile is assumed to be made of one or more perfectly bonded dissimilar layers or disks. Upon impact, shock waves are set up in the projectile and target materials. The pressures associated with these shocks typically exceed the strengths of the projectile and target materials by several orders of magnitude. As the shock waves propagate, the projectile and target materials are heated adiabatically and nonisentropically. The release of the shock pressures occurs isentropically through the action of rarefaction waves that are generated as the shock waves interact with the free surfaces of the projectile and target. This process leaves the projectile and target materials

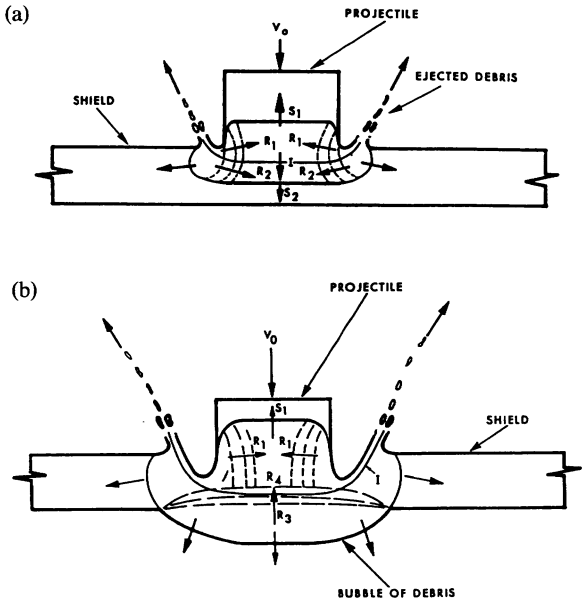

(b) After the Shock in the Shield Has Reflected From the Bottom Face of the Shield

FIGURE 1 Wave patterns in a projectile and an impacted target (Maiden et al., 1963).

in high energy states and can cause either or both to fragment, melt, or vaporize, depending on the material properties, geometry, and the impact velocity.

At very early times during the impact event, only the area in the immediate vicinity of the impact site is affected by the impact. For the projectile and target geometries considered in this study, the shock waves can be considered to be initially planar. This simplification allows one-dimensional relationships to be used for analyzing the creation and release of shock pressures. The shock pressures, energies, etc., in the projectile and target materials are calculated using the three one-dimensional shock-jump conditions, a linear relationship between the shock wave velocity and particle velocity in each material, and continuity of pressure and velocity at the projectile–target interface. Solving the resulting equations simultaneously yields expressions for projectile and target particle velocities that are then used to calculate shock velocities, pressures, internal energies, and material densities after the passage of a shock wave.

Although the shock loading of a material is an irreversible process that results in an increase of the internal energy of the shocked material, the release of a shocked material occurs isentropically along an "isentrope" or "release adiabat." The difference between the area under the isentrope and the energy of the shocked state is the amount of residual energy that remains in the material and can cause the material to melt or even vaporize. To calculate the release of the projectile and target materials from their respective shocked states, an appropriate equation-of-state is needed for each material. To keep the analysis relatively simple, the Tillotson equation-of-state was used in this study (Tillotson, 1962).

Propagation of Shock Pressures in a Multimaterial Projectile

As the shock wave generated by the impact on the target propagates through a multimaterial projectile, it encounters the various interfaces between material layers. At each interface between two dissimilar materials, a transmitted shock wave and a reflected wave are generated. The properties of the reflected and transmitted waves are found using the method of impedance matching (see, e.g., Rinehart, 1975). In this technique, continuity of pressure and particle velocity are enforced at each interface. If the reflected pressure is greater than the incident pressure, then the reflected wave is a shock wave. Conversely, if the reflected pressure is less than the incident pressure, the reflected wave is a rarefaction wave. Once the pressure and the particle velocity in a subsequent material layer are determined, the one-dimensional shock-jump conditions are used to calculate the specific volume and the energy of the shocked material. This procedure is repeated for each successive projectile material layer. Thus, the impact conditions are used to define the shocked states in the target and first projectile layer materials; the shocked states in subsequent projectile material layers are obtained using an impedance matching technique.

Release of Shock Pressures

The target shock pressures are released by the action of the rarefaction wave that is created by the reflection of the shock wave in the target from the target rear free surface (R_3 in Fig. 1). This rarefaction wave propagates through the target material and into the shocked projectile layer materials. In doing so, it also releases the projectile materials from their respective shocked states. For the purposes of the model developed herein, this process of shocking and releasing continues until the rarefaction wave overtakes the shock wave. After this point in time, it is assumed that no additional shocking and release of projectile material occurs. In this manner, the model developed herein considers only material that is "fully shocked."

As mentioned previously, in some instances the relative impedance of two adjoining projectile layer materials may result in a shock wave being reflected back into a projectile material layer that has been shocked and released. However, it is assumed for the purposes of this study that this reflected shock wave does not "reshock" the projectile material and that the material into which it is reflected remains released. This assumption is reasonable because as the reflected shock wave moves back into the released layer material, it continuously creates rarefaction waves at the projectile edge free surfaces that release any material shocking it produces. Thus, in this model, any projectile layer material that has been shocked and released will remain released regardless of the nature of the wave reflected from its interface with an adjoining layer.

DEBRIS CLOUD MATERIAL CHARACTERIZATION

Computing Percentages of Solid, Liquid, and Gaseous Debris Cloud Material

Once the residual internal energies in the shocked and released portions of the projectile and target materials are obtained, the percentages of the various states of matter in the resulting debris cloud are estimated using the following procedure. This procedure requires the knowledge of the materials' solid and liquid specific heats (C_{ps}, C_{pl}), melting and boiling points (T_m, T_v), and heats of fusion and vaporization (H_f, H_v) in addition to the residual internal energy (E_r).

If $E_r < C_{ps}T_m$, all of the shocked and released materials is considered to remain in a solid matter state. If $C_{ps}T_m < E_r < C_{ps}T_m + H_f$, the quantity $(E_r - C_{ps}T_m)/H_f$ represents the fraction of the shocked and released material that was melted, while the remaining shocked and released material is assumed to be in solid form. If $C_{ps}T_m + H_f < E_r < C_{ps}T_m + H_f + C_{pl}(T_v - T_m)$, all of the shocked and released material is considered to be in a liquid state. If $C_{ps}T_m + H_f + C_{pl}(T_v - T_m) < E_r < C_{ps}T_m + H_f + C_{pl}(T_v - T_m) + H_v$, the quantity $\{E_r - [C_{ps}T_m + H_f + C_{pl}(T_v - T_m)]\}/H_v$ represents the fraction of the shocked and released material that was vaporized, while the remaining shocked and released material is considered to be in liquid form. If $C_{ps}T_m + H_f + C_{pl}(T_v - T_m) + H_v < E_r$, all of the shocked and released material is vaporized.

Computing Masses of Solid, Liquid, and Gaseous Debris Cloud Material

The material in the debris cloud created by the initial impact consists of the target material removed by the impact and the impacting projectile mass. The mass of the projectile material in the debris cloud is known a priori; the mass of the target material in the debris cloud is determined by multiplying the target hole-out area by the target thickness and the target material density. The diameter of the hole created in the target plate by the initial impact can be calculated using any one of a number of empirical equations for hole diameter in a thin plate due to a high speed impact (see, e.g., Jolly, 1993).

To calculate the masses of the various states of the projectile and target materials in the debris cloud, the amounts of shocked and released target and projectile material must be determined. Referring to Figure 1, these quantities are obtained by determining the location in the target plate where the rarefaction wave R_2 overtakes shock wave S_2 (Maiden et al., 1963). In the projectile, the rarefaction and shock waves of interest are R_4 and S_1, respectively. It is the material through which both the shock wave and the release wave travel that is shocked and released and is therefore either melted or vaporized, depending on the particulars of the impact event. Any material beyond the point at which the rarefaction wave overtakes the shock wave is assumed, for the purposes of this study, not to be shocked and to remain in a solid matter state. If the point at which the release wave overtakes the shock wave is beyond the thickness of the target plate or the length of the projectile, then all of the material is considered shocked and released. For the target plate and for a single-material projectile, the equations derived by Maiden et al. (1963) are used directly. For a multimaterial projectile, the location in the projectile where the rarefaction wave overtakes the shock wave is determined using a technique based on that used for a single-material projectile.

Consider Figure 2, which is an extension of the single material projectile curves to the case of a multimaterial projectile. In Figure 2, the speeds of the waves R_4 and S_1, which are denoted by D and E subscripts, respectively, are seen to change as they move through the projectile material layers. In addition, the interface velocity, which is denoted by a C subscript, also changes from interface to interface due to the different material layer properties. As in the case of a single-material projectile, we are interested in calculating the length L_4, which is the distance from

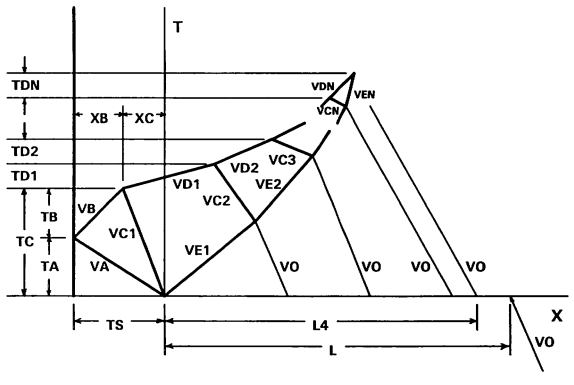

FIGURE 2 Extension of single-material X-T diagram to multimaterial projectiles.

the undisturbed leading edge of the projectile to the point within the projectile where the rarefaction wave R_4 overtakes the shock wave S_1 as it moves through the various projectile layers. This quantity is obtained by performing a sequence of calculations provided by Schonberg (1994).

Figure 3 shows the results obtained when these calculations are applied to a three-layer projectile impacting an aluminum plate at 6 km/s. The projectile materials, their stacking sequence, and the geometry of the impact are also given in Figure 3. As can be seen from Figure 3, the original rarefaction wave emanating from the target rear surface overtakes the shock wave in the projectile at a distance of approximately 0.71 cm from the leading edge of the undisturbed projectile. This implies that at the impact velocity considered, the first two projectile layers (i.e. the aluminum and the steel) are completely shocked and released as is the first 0.202 cm of the third projectile layer (i.e. the tungsten).

In calculating the amount of target material subject to shock loading and release, it is assumed that the shocked target material comes from an area of the target equal to the presented area of the projectile (Herrmann and Wilbeck, 1987); the remaining material ejected from the target in the creation of the target plate hole is assumed to remain in a solid, albeit undoubtedly fragmented, state. Further, it is also assumed that the depth of the shocked target material extends completely through the target thickness. Were this not the case, then other target failure modes, such as plugging, for example, might come into play. This in turn would seriously compromise the validity of the assumptions made in the development of this debris cloud model. A direct consequence of this assumption is that this model is not valid for "thick" target plates.

Once the projectile and target mass contributions to the debris cloud and the fractions of these masses that were shocked and released were obtained, the masses of the target and projectile materials in each of the three states of matter are computed by multiplying each matter state percentage by the appropriate total shocked and released mass. The mass of the solid shocked and released material (if any) is then added to the mass of the unshocked material (if any) to obtain the total mass of the solid component of the debris cloud material.

Debris Cloud Velocities

The equations developed in the subsequent sections are presented in their most general form. They can be applied directly to a single-material projectile and adapted easily to the impact of a multimaterial projectile. In characterizing the velocities of the debris cloud created by a hypervelocity impact on a thin plate, there are two possibilities that need to be considered.

First, all of the projectile material is shocked and released. In this case, the debris cloud consists of the projectile and target material that is

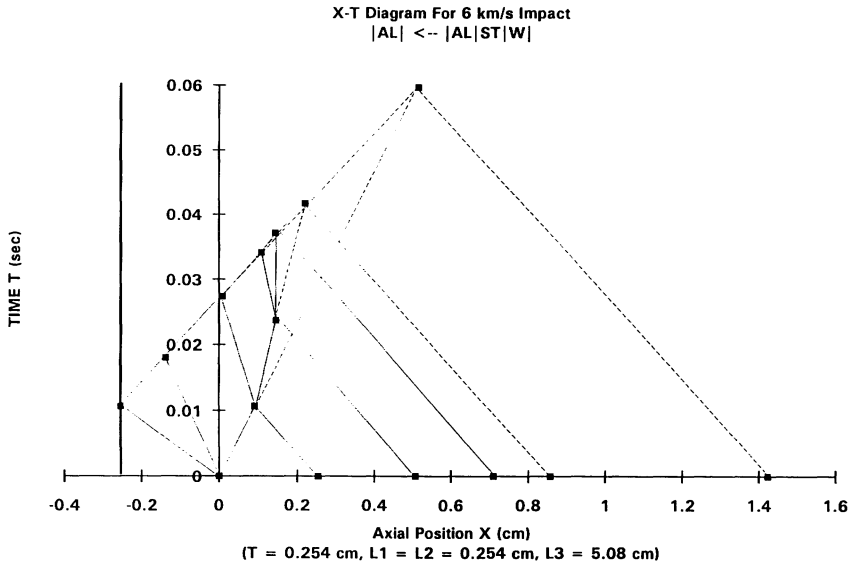

FIGURE 3 Movement of rarefaction wave R_4 and shock wave S_1 specific example.

shocked and released and the additional fragmented target material that is ejected from the target plate during the perforation process but, according to the assumptions made herein, is not shocked and released. In the debris cloud model developed herein, all of this material is allowed to move axially and expand radially. The quantities of interest in this case are therefore the debris cloud leading edge, center-of-mass, trailing edge, and expansion velocities, that is, v_f, v_i, v_r, and v_{exp}, respectively.

Second, some of the projectile material remains, according to the assumptions employed herein, unshocked. Although it would not be appropriate to call this unshocked projectile material a "residual projectile mass," it is reasonable to presume that this material is less severely stressed than that which is fully shocked and then released. Hence, it is also reasonable to presume that if there is any unshocked projectile material, then it does not significantly expand radially as it moves axially. In this case, the debris cloud consists of shocked and released target and projectile materials and the additional unshocked fragmented target material. The quantities of interest are the debris cloud leading edge, center-of-mass, and expansion velocities (v_f, v_i, and v_{exp}) and the velocity of the remaining unshocked projectile material, v_{pr}. Note that due to the presence of the unshocked projectile mass, there is no debris cloud trailing edge for which to calculate a velocity.

Debris Cloud Velocity and Spread Calculations. Consider the impact of a projectile on a thin target and the debris cloud created by it as shown in Figure 4. As indicated in the figure, the velocities of interest are v_f, v_i, v_{exp}, and v_r. As the initial shock wave created by the impact strikes the rear surface of the target, it creates a rarefaction wave that travels back into the target and eventually in some form into the projectile. This action and interaction of the shock wave and the free surface impacts a velocity u_{fst} to the target rear surface equal to the sum of the particle velocity in the target material due to the shock wave u_{pt} and the particle velocity due to the rarefaction wave u_{rt}, that is,

$$u_{fst} = u_{pt} + u_{rt}. \tag{1}$$

Because $u_{rt} \approx u_{pt}$ (Rice et al., 1958), we simply have $u_{fst} = 2u_{pt}$.

In both of the cases described in the previous subsection, the velocity of the leading edge of the debris cloud v_f is approximated with u_{fst} (see also Piekutowski, 1990), that is,

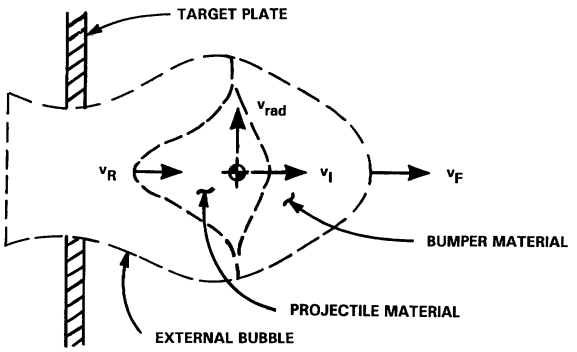

FIGURE 4 Debris cloud velocities.

$$v_f = u_{fst} = 2u_{pt}. \tag{2}$$

Also common to both cases is that the half-angle measuring the spread of the debris cloud materials is given by

$$\theta = \tan^{-1}(v_{exp}/v_i). \tag{3}$$

What distinguishes the two types of debris clouds mathematically is the manner in which v_i, v_{exp}, and v_r or v_{pr} are calculated. When all of the projectile material is shocked and released, then:

$$v_r = v_o - u_{fsp}; \tag{4}$$

v_i is obtained from momentum conservation before and after the impact event, that is,

$$v_i = m_p v_o / m_{dc}; \tag{5}$$

and, v_{exp} is obtained from the application of energy conservation before and after the impact event, that is,

$$m_p v_o^2/2 = E_{pr} + E_{tr} + m_{dc} v_i^2/2 + m_{dc} v_{exp}^2/2 \tag{6}$$

where $m_{dc} = m_p + m_t$ is the total debris cloud mass; m_p is the projectile mass; m_t is the total target hole-out mass; E_{pr} and E_{tr} are the internal projectile and target energies, respectively, that have gone into heating the projectile and target materials; and $u_{fsp} = u_{pp} + u_{rp}$ is the velocity of the rear free surface of the projectile. As in the case of u_{fst}, u_{fsp} is taken to be equal to the sum of the particle velocity in the projectile material due

to the passage of the shock wave, u_{pp}, and the particle velocity due to the passage of the rarefaction wave in the projectile material, u_{rp}, created by the reflection of the shock wave from the projectile rear free surface.

In the event when not all of the projectile material is shocked and released, then v_i, v_{exp}, and v_{pr} are obtained through the solution of the following three simultaneous equations:

$$v_{exp} = v_f - v_i; \tag{7}$$

$$m_p v_o = m_{pr} v_{pr} + m_{dc} v_i; \tag{8}$$

$$m_p v_o^2/2 = E_{pr} + E_{tr} + m_{pr} v_{pr}^2/2 + m_{dc} v_i^2/2 + m_{dc} v_{exp}^2/2 \tag{9}$$

where in this case $m_{dc} = m_p + m_t - m_{pr}$, and m_{pr} is the mass of the unshocked projectile material. In this particular case, substituting for v_{exp} and v_{pr} into eq. (9) using appropriate expressions obtained from eqs. (7) and (8) yields a quadratic equation for v_i. This equation is then solved to yield the following expression for v_i:

$$v_i = b/a - [(b/a)^2 - (c/a)]^{1/2} \tag{10}$$

where

$$a = 2 + m_{dc}/m_{pr} \tag{11a}$$

$$b = v_f + (m_p/m_{pr}) v_o \tag{11b}$$

$$c = v_f^2 + (m_p/m_r - 1)(m_p/m_{dc}) v_o^2 + 2(E_{pr} + E_{tr})/m_{dc}. \tag{11c}$$

The quantities v_{exp} and v_{pr} are then easily obtained from eqs. (7) and (8).

DEBRIS CLOUD CHARACTERIZATION SCHEME VERIFICATION

A FORTRAN program called DEBRIS3 (Schonberg, 1994) was written to implement the various equations and procedures described previously. DEBRIS3 is an interactive program that prompts the user for the following information:

1. number of projectile layers;
2. projectile material;
3. target material;
4. impact velocity;
5. target thickness;
6. projectile diameter;
7. lengths of projectile layers; and
8. hole diameter option.

DEBRIS3 requires a material library input file, which also contains appropriate Tillotson equation-of-state parameters. DEBRIS3 generates an output file, which contains a detailed summary of the following information:

1. projectile and target geometric and material properties;
2. impact conditions;
3. projectile and target material equation-of-state parameters;
4. projectile and target material end-state calculation results, including the waste heat generated, the resulting temperature increase, the percent of solid, liquid, and vaporous material, and the masses of the solid, liquid, and vaporous components; and
5. debris cloud velocities v_f, v_i, and v_r, and v_{exp}, as applicable.

In the following two sections, the predictions of DEBRIS3 are compared qualitatively and quantitatively against experimental results, the predictions of various one- and three-dimensional hydrocodes, and the predictions of several empirically based lethality assessment schemes. For single-material projectiles, direct quantitative comparisons are possible because of the availability of experimental and numerical data for the chosen projectile geometry. Unfortunately, quantitative comparisons with experimental results for multimaterial projectiles are not possible because such data does not exist in the open literature for cylindrical projectiles. However, qualitative comparisons with experimental results were still possible using the results of a series of impact tests performed with layered spherical projectiles. In an attempt to lend further credibility to the model developed herein, a series of CTH runs was performed using layered cylindrical projectiles. This allowed a direct quantitative assessment of the predictions of DEBRIS3 for multimaterial projectiles.

Single-Material Projectiles

Comparison with Experimental Results and One-Dimensional Hydrocode Predictions. Debris cloud velocity values were calculated using DEBRIS3 and compared against experimental

results and one-dimensional hydrocode predictions obtained from a previous study of debris cloud formation and growth using thin copper disks ($L/D = 0.3$) impacting thin aluminum plates (Piekutowski, 1990). As can be seen in Table 1, the predictions of DEBRIS3 for v_f, v_i, and v_r were in excellent agreement with those of the one-dimensional hydrocode and the experimental results.

Over all the cases considered, the average difference between the predictions of DEBRIS3 for v_f, v_i, and v_r and the corresponding experimental results was approximately 4% with a standard deviation of approximately 3%. However, the predictions of DEBRIS3 for v_{exp} exceeded the experimental results by an average of approximately 40% with a standard deviation of approximately 15%. This discrepancy may have been due to the fact that the expansion velocity measured by Piekutowski (1990) was that of the heavier copper component of the debris cloud while the velocity calculated by DEBRIS3 was based on both debris cloud materials.

Comparison with CTH and Lethality Assessment Scheme Predictions. Figure 5 presents a comparison of the predictions of DEBRIS3, the hydrocode CTH, and the semiempirical code FATEPEN2 (Yatteau et al., 1991a, b) for debris cloud leading edge velocity v_f for steel cylinders ($L/D = 1$) normally impacting thin aluminum target plates ($T/D = 0.125$). As is evident in Figure 5, the predictions of DEBRIS3 compare favorably with those of FATEPEN2 in the velocity regime for which FATEPEN2 was designed to be used (i.e. less than approximately 5 km/s). A quick calculation reveals that the difference between the DEBRIS3 predictions of leading edge velocity and those of FATEPEN2 was approximately 26% of the DEBRIS3 values with a standard deviation of approximately 4% for the impact velocities considered. One reason for this difference could be the fact that the mass of the impacting projectile considered exceeded the maximum value of projectile masses used to develop the FATEPEN2 equations.

The CTH values plotted in Figure 5 are average values of the velocities of three Lagrangian station points along the impact centerline within the aluminum target plate. These average values differed from the corresponding minimum and maximum values by approximately 0.5 km/s at an impact speed of 2 km/s and 3.0 km/s at an impact speed of 14 km/s. Inspection of Figure 5 also reveals that there is excellent agreement between the predictions of DEBRIS3 and CTH for debris cloud leading edge velocity. The average difference between the DEBRIS3 and CTH values was approximately 4% of the DEBRIS3 values with a standard deviation of approximately 3%.

Figure 6 presents a comparison of the predictions of DEBRIS3, CTH, FATEPEN2, and two other semiempirical damage assessment codes, PEN4 (Bjorkman et al., 1987) and KAPP-II (Greer and Hatz, 1992), for debris cloud half-an-

Table 1. Comparison of DEBRIS3 with Empirical Results and 1-D Hydrocode Predictions

T	m_p	v_o	v_f/v_o			v_i/v_o			v_r/v_o			v_{exp}/v_o	
(mm)	(g)	(km/s)	(1)	(2)	(3)	(1)	(2)	(3)	(1)	(2)	(3)	(1)	(3)
Effect of Target Thickness													
1.0	1.0	6.39	1.44	1.41	1.40	0.91	0.89	0.89	0.36	0.34	0.34	0.24	0.27
1.5	1.0	6.36	1.44	1.41	1.40	0.88	0.83	0.84	0.36	0.34	0.34	0.24	0.32
2.0	1.0	6.38	1.42	1.41	1.40	0.83	0.79	0.79	0.35	0.34	0.33	0.27	0.36
2.5	1.0	6.53	1.46	1.41	1.40	0.79	0.76	0.75	0.35	0.34	0.33	0.27	0.38
Effect of Impact Velocity													
1.5	1.0	3.45	1.37	1.39	1.39	0.86	0.84	0.84	0.43	0.36	0.36	0.23	0.33
1.5	1.0	4.85	1.43	1.40	1.39	0.87	0.84	0.84	0.39	0.35	0.35	0.23	0.33
1.5	1.0	6.36	1.44	1.41	1.40	0.88	0.83	0.84	0.36	0.34	0.34	0.24	0.32
Effect of Projectile Mass													
2.0	1.0	6.38	1.41	1.41	1.40	0.83	0.79	0.79	0.35	0.34	0.34	0.27	0.36
2.9	3.0	5.66	1.44	1.40	1.40	0.82	0.80	0.79	—	0.34	0.34	0.23	0.36
4.4	10.0	5.12	1.40	1.40	1.39	0.83	0.80	0.79	0.36	0.35	0.35	0.22	0.37

(1) Experimental Results (Piekutowski, 1990).
(2) 1-D Hydrocode Predictions (Piekutowski, 1990).
(3) DEBRIS3 Predictions.

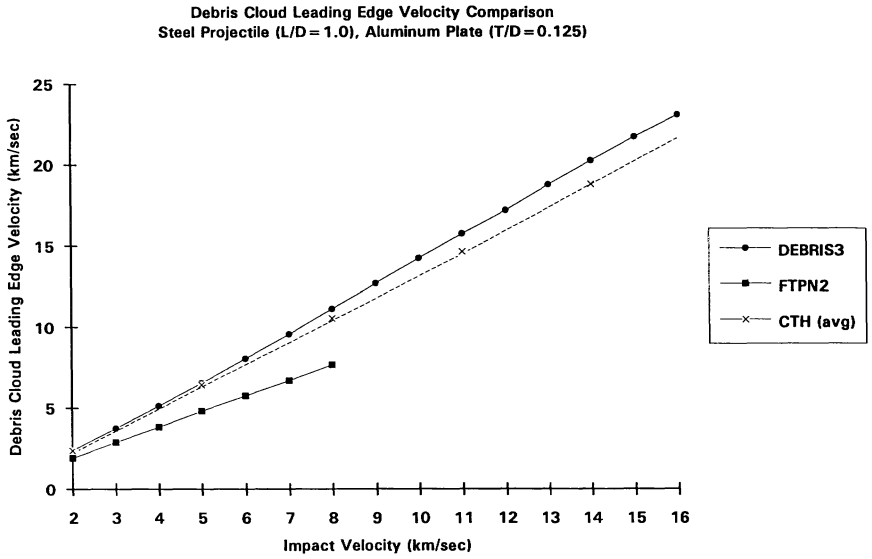

FIGURE 5 Debris cloud leading edge velocity comparisons.

gle for steel cylinders (L/D = 1.0) normally impacting thin aluminum target plates (T/D = 0.125). In Figure 6, the average difference between the predictions of KAPP-II and DEBRIS3 was approximately 18% of the DEBRIS3 value with a standard deviation of approximately 10%; the average difference between PEN4 and DEBRIS3 was approximately 6% with a standard deviation of nearly 7%. Based on these results, it may be argued that the predictions of DEBRIS3 agree fairly well with those of KAPP-II and PEN4. However, comparing the differences between DEBRIS3 and FATEPEN2 was somewhat more difficult because FATEPEN2 distinguishes between target debris spread and projectile debris spread but DEBRIS3 does not. In FATEPEN2, the target debris half-angle is fixed at 25° while the projectile debris half-angle is based on material properties, impact conditions, etc.

It is interesting to note that unlike the smooth curve predictions of KAPP-II, FATEPEN2, and PEN4, the curve representing the growth of the debris cloud spread generated by DEBRIS3 contains numerous kinks. In particular, the impact

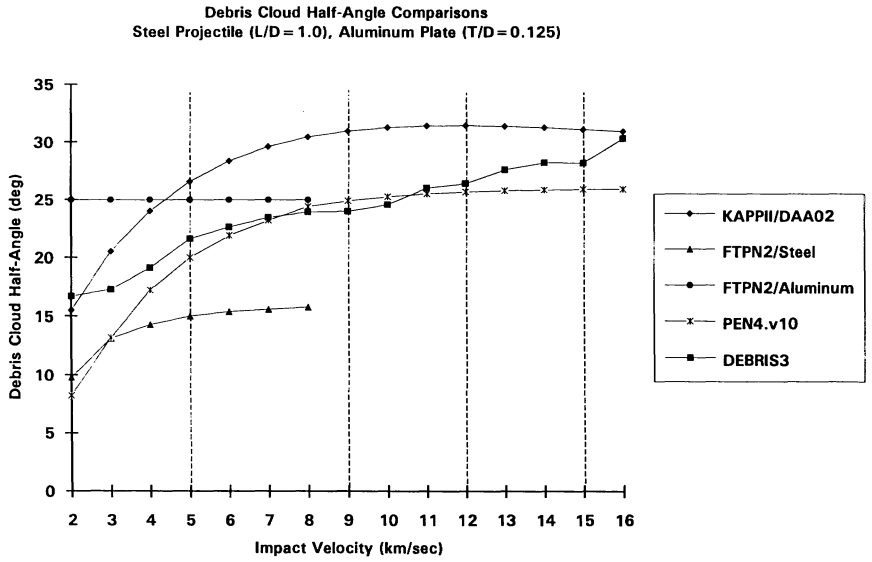

FIGURE 6 Debris cloud half-angle comparisons.

velocities corresponding to the vertical lines in Figure 6 also correspond to impact velocities at which significant changes occur in the way the initial kinetic energy of the projectile is distributed to various competing mechanical and thermal processes during the impact event. These features of the curve predicted by DEBRIS3 are discussed in the following paragraph.

For the impact considered in Figure 6, between 2 and 5 km/s, increasing the impact velocity resulted in a steady increase in debris cloud spread. However, at 5 km/s, the target material began to melt. As a result, some of the additional kinetic energy of the initial impact provided as impact velocity increased beyond 5 km/s was used up by the target material state change and was not available for debris cloud expansion. Thus, the rate of debris cloud expansion slowed, and the slope of the curve decreased as impact velocity increased beyond 5 km/s. Between 8 and 9 km/s, the projectile material began to melt and the target material began to vaporize. This further decreased the rate of debris cloud expansion. However, once the projectile was completely melted, the rate of debris cloud expansion increased. Near 12 km/s, the projectile material began to experience vaporization. The rate of debris cloud expansion slowed down only slightly because by now the debris cloud consisted of a significant amount of hot vaporous material. By 15 km/s, the debris cloud was nearly all vapor causing its rate of expansion to increase dramatically.

Multimaterial Projectiles

Comparison with Experimental Results. Three high speed impact tests were performed at 4 km/s using three different equal-weight projectiles (Wilbeck et al., 1988). The first was a solid 7.5-g TA10W (i.e. a tantalum alloy with 10% tungsten) sphere, while the second and third projectiles were 7.5-g layered spheres with a solid TA10W core surrounded by a steel shell. The outer shell of the second projectile was 1018 steel (i.e. mild strength steel) and that of the third projectile was 4340 steel (i.e. a high strength steel).

In simulating these three impact tests with DEBRIS3, the layered spheres were modeled as cylindrical projectiles with three layers. The middle layer corresponded to the spherical core and the first and third layers represented the outer shell material. The thicknesses of the first and third layer were set equal to the outer shell thickness. The thickness of the inner layer and the diameter of the cylindrical projectile were calculated by setting the inner layer thickness equal to the cylindrical projectile diameter and then solving for the diameter by equating the mass of the cylindrical projectile to the mass of the original layered sphere.

In addition to adapting the geometry of the original projectiles used in the test series to a projectile geometry that was compatible with DEBRIS3, some compromises were also made regarding the projectile and target materials. In the original test series, the target was a two-dimensional flat plate representation of a half-scale reentry vehicle, that is, a layer of silica phenolic bonded to a thin layer of aluminum. Because the current version of DEBRIS3 does not allow for multimaterial targets, the targets used in the DEBRIS3 impact simulations did not have the outer layer of silica phenolic. In addition, whereas one of the original projectile materials was a tantalum alloy with 10% tungsten, the corresponding material in the DEBRIS3 impact simulations was pure tantalum.

As expected, the simplifications described in the previous two paragraphs precluded any direct comparison of the predictions of DEBRIS3 and the experimental results. However, it was possible to make qualitative comparisons of the DEBRIS3 predictions and the actual test results because the simplifications maintained some similarity between the original test materials and configurations and the materials and geometries of the DEBRIS3 impact simulations. These qualitative comparisons became possible after the DEBRIS3 predictions were analyzed to infer the relative severity of the damage levels that could have been expected on subsequent witness plates had they been placed behind the initial target plate.

First, DEBRIS3 predicted that a significant portion of the target material would be melted when impacted by the solid tantalum sphere. Alternatively, when impacted by the layered projectiles, DEBRIS3 predicted that the target material would be shocked and released but would return to a solid state of matter. This indicates that the target material would probably be fragmented but not melted. Second, DEBRIS3 predicted that the kinetic energy of the remaining unshocked projectile material would be greatest for the layered projectile with a tantalum core and a high-strength steel shell and would be least for the solid tantalum projectile. Taken together,

these two features indicate that the cylindrical projectiles simulating the layered sphere projectiles would probably inflict more severe damage on a witness plate behind the target than would the cylindrical projectile simulating the solid TA10W projectile. This agrees with the actual test results that state that among the three impact tests, the crater depth and volume in a witness block behind the target impacted by the projectile with a TA10W core and a 4340 steel shell were greatest and those in a block behind the target impacted by the solid TA10W projectile were least.

Comparison with Hydrocode Predictions: First Series. The first series of numerical runs consisted of two sets of three high speed impacts at 11 km/s using the SOIL hydrocode (Wilbeck et al., 1988). The projectiles used were similar in construction to those in the previously discussed experimental tests (i.e. one solid and two layered spheres in each test set). The major distinguishing feature between the two sets of impact simulations in this series is the mass of the projectiles: 45-g projectiles were considered in the first set; 5-g projectiles were used in the second set. In both sets of simulations, the solid sphere was made out of tungsten as was the core in the layered spheres; the shells of the layered spheres were made out of different strength steels. In modeling the SOIL impact simulations with DEBRIS3, simplifications in the projectile and target geometries were made similar to those in the previous section. As a result, the following comparisons are again only qualitative in nature.

As in the DEBRIS3 simulations of the experimental tests, the DEBRIS3 simulations of the SOIL runs indicated that the solid projectiles would melt some of the target plate material but the layered projectiles would not. In addition, the kinetic energies of the unshocked projectile materials from the layered projectiles greatly exceeded those of the unshocked projectile materials from the solid projectiles. These two features again indicate that the layered projectiles would inflict more severe damage on a witness plate behind the target than would an equal-weight solid projectile.

Interestingly enough, while the general trends observed in the DEBRIS3 impact simulations agreed with the hypothesis that motivated the original layered projectile investigation, they disagree with the actual numerical results obtained as part of that investigation. The corresponding SOIL runs predicted that the witness block damage due to the impacts of the solid projectiles would be approximately the same as the damage caused by the layered projectiles. Apparently, either the impact and/or geometric parameters used in the SOIL runs masked subtle differences in damage levels resulting from the solid and layered projectile impacts and prevented them from being discernible, or the DEBRIS3 modeling of the projectile and target geometries overemphasized some impact phenomenology that produced some differences in response that would otherwise have been negligible.

In any event, it is apparent that additional testing of multimaterial projectiles that are compatible with the modeling capabilities of DEBRIS3 are required to fully validate the predictive capabilities of DEBRIS3. As an intermediate step, several CTH runs were performed using projectile and target geometries that were ideally suited for and matched to the capabilities of DEBRIS3. The results of these runs and how they compared with the predictions of DEBRIS3 are discussed in the next section.

Comparison with Hydrocode Predictions: Second Series. In the second series of hydrocode runs, four higher speed impact simulations were performed at 10 km/s using CTH with multimaterial cylindrical projectiles. The projectile diameter and target plate thickness were kept constant at 2.54 and 0.3175 cm, respectively. In the first two runs, the layers were relatively "thin" (i.e. $L/D = 0.1$ each); in the second two runs, the projectile layers were relatively "thick" (i.e. $L/D = 1.0$ each). In the first and third runs, an aluminum target plate was impacted by a projectile with an aluminum leading layer, a 4340 steel middle layer, and a tungsten rear layer. In the second and fourth runs, the order of the projectile materials was reversed. A detailed description of the impact and geometric parameters are given in Table 2; the results of the DEBRIS3 impact simulations and the corresponding CTH results are given in Table 3. In Tables 2 and 3, a 1 in the first column refers to the leading layer of the projectile and a 3 refers to the rear-most projectile layer.

The predictions of CTH and DEBRIS3 regarding the state of the target and projectile layer materials were compared quantitatively and qualitatively. To facilitate quantitative comparisons of material end states, average densities were computed for each material layer using the

Table 2. Geometric and Impact Parameters for DEBRIS3 and CTH Comparison Runs

	Run No.			
	(1)	(2)	(3)	(4)
V (km/s)	10.0	10.0	10.0	10.0
D (cm)	2.54	2.54	2.54	2.54
T (cm)	3.175	3.175	3.175	3.175
Material				
Target	Aluminum	Aluminum	Aluminum	Aluminum
Layer 1	Aluminum	Tungsten	Aluminum	Tungsten
Layer 2	4340 Steel	4340 Steel	4340 Steel	4340 Steel
Layer 3	Tungsten	Aluminum	Tungsten	Aluminum
L_1 (cm)	0.254	0.254	2.54	2.54
L_2 (cm)	0.254	0.254	2.54	2.54
L_3 (cm)	0.254	0.254	2.54	2.54
L/D	0.3	0.3	3.0	3.0
Proj. mass (g)	38.24	38.24	382.40	382.40

DEBRIS3 and CTH results. The DEBRIS3 values were obtained by multiplying the mass of shocked and released material by its final density, adding to it the product of the density of the unshocked material and its mass, and then dividing by the total mass of the material layer under consideration. The CTH values are simply average values through the particular layer thickness and were obtained from density history plots along the centerline.

A feature common to all four impact simulations and evident in Table 3 is that the average target material densities predicted by DEBRIS3 were significantly higher than those predicted by CTH. However, the reason for this is that they include the solid component of target material not considered to be shocked and released by the impact (i.e. the remainder of the ejected target material not swept out by the projectile). The contributions of the solid material component to the average density of the target material are significant considering that they constitute approximately 90% of the target material in the debris cloud created by the impact. If the target hole diameter had been set equal to the projectile diameter (which is not an unreasonable assumption for the impact velocity and geometries considered), then there would not have been any unshocked target material and it is reasonable to presume that the average densities of the target material would have been much closer to the CTH values.

The differences between the DEBRIS3 predictions of debris cloud leading edge velocity and the corresponding CTH values in runs 1–4 are 25.4, 22.3, 3.9, and 13.9%, respectively, of the CTH values. The somewhat large differences in runs 1 and 2 may be explained by the following

Table 3. Comparison of DEBRIS3 and CTH Impact Response Predictions

	Run No.							
	(1)		(2)		(3)		(4)	
	DEBRIS3	CTH	DEBRIS3	CTH	DEBRIS3	CTH	DEBRIS3	CTH
V_f (km/s)	10.65	14.27	17.36	14.20	10.65	11.08	16.26	14.28
θ (deg)	36	32	34	27	48	37	21	22
ρ_{targ} (g/cm^3)	2.56	0.21	2.36	~0.0	2.63	1.33	2.52	~0.0
ρ_1 (g/cm^3)	2.02	~0.0	18.52	0.67	2.22	2.25	18.98	9.20
ρ_2 (g/cm^3)	7.04	0.17	7.25	5.50	7.83	8.53	7.83	6.94
ρ_3 (g/cm^3)	18.42	0.97	2.48	1.41	19.17	17.19	2.71	3.39

considerations. In the characterization scheme employed by DEBRIS3, the target shock loading and release analysis used to obtain the debris cloud leading edge velocity is truly one-dimensional, that is, it is performed using only the leading projectile layer and the target material. Anything behind the first projectile material layer is ignored. In the case of thick projectile layers, the use of one-dimensional equations is appropriate because the rear layers of the projectile are sufficiently far from the impact site to not affect the magnitude of the velocity of the target rear free surface. However, in the case of the thin projectile layers, the second and third projectile layers are close enough to the projectile–target interface to influence the shock and release process in the target material and the resulting velocity of the target rear free surface. CTH, being a three-dimensional hydrocode, is apparently sensitive to these effects while DEBRIS3, being a first principles based code, is not. As a result, the CTH and the DEBRIS3 predictions differ somewhat more in runs 1 and 2 and are more in agreement in runs 3 and 4.

The differences between the DEBRIS3 predictions of debris cloud leading edge velocity and the corresponding CTH values in runs 1–4 are 11, 26, 23, and 5%, respectively, of the DEBRIS3 values. The CTH predictions of debris cloud half-angle were obtained indirectly from debris cloud output plots. In some cases, the precise angles were difficult to determine from the CTH plots because not all of the debris cloud material was retained by CTH and subsequently plotted. If there is a very small fraction of a material in a cell in which more than one material is present, then it is possible for that small fraction of material to generate negative internal energies in that cell. CTH allows the user to set a flag that forces CTH to drop the cell from subsequent calculations in such cases. If this is not done, then in such cases the time step becomes so small that the impact simulation will be forced to terminate prematurely. Apparently, in runs 2 and 3, CTH dropped a fair amount of cells as the calculations proceeded that in turn produced rather sparse debris clouds. Although the agreement between the DEBRIS3 predictions and the CTH values was in general fairly reasonable, this may explain in part why in runs 2 and 3 the DEBRIS3 predictions of the half-angle values were significantly higher than the CTH values.

For projectiles with thin layers, although Table 3 indicates that there were significant differences between the material densities predicted by DEBRIS3 and those obtained with CTH, closer examination of the DEBRIS3 and CTH predictions of material state did in fact reveal a qualitative agreement in the results. For example, the extremely low material densities for run 1 predicted by CTH indicate that the material from the three projectile layers in both cases are in highly expanded states. However, the density of the rear-most portion of the third material layer in run 1 (approximately the last 33%) was nearly 3.5 times that of the forward portion of that layer, indicating that the rear third of the final projectile layer was significantly more dense than the rest of the projectile material. Interestingly enough, for run 1, DEBRIS3 predicted that the first two material layers would be in a liquid state, while the last 25% of the third layer would not be fully shocked. Thus, although the actual density values may have been different (which was not totally unexpected given the relatively simple nature of the physics employed by DEBRIS3), there was some qualitative agreement between CTH and DEBRIS3 with regard to the state of the projectile material following the initial impact.

With regard to the target material, CTH predicted that the target material would be in a highly expanded state in run 1 and probably vaporized in run 2; DEBRIS3 predicted that the target material would be completely melted in run 1 and in run 2 it would be partially vaporized as well. Thus, there was again some general agreement between CTH and DEBRIS3 regarding the state of the target material following a hypervelocity impact of a projectile with thin material layers.

For projectiles with thick material layers, projectile material characterizations predicted by DEBRIS3 were again found to agree in a general sense with the postimpact material states predicted by CTH (Table 3). For example, DEBRIS3 predicted in both run 3 and run 4 that the second and third projectile layers would remain unshocked while part of the first layer would be shocked and released. The CTH results for runs 3 and 4 showed the third material layers to be relatively undisturbed and the second material layers to be only slightly deformed. These characteristics are also evident in Table 3 where the density values predicted by CTH for the second and third projectile material layers were near ambient values; the densities predicted by DEBRIS3 for the second and third layers were

naturally exactly equal to the respective ambient values due to the assumptions within the DEBRIS3 model.

With regard to the first material layer, DEBRIS3 predicted that in run 3 the entire shocked and released portion would be all liquid, and the shocked and released portion in run 4 would be a mixture of liquid and solid material. The CTH results for both cases showed that the density of the leading edge of the first layer was approximately 30% of the ambient value, while the density of the rear portion of the leading layer approached the ambient value of the second layer material, indicating a significantly more compressed state than that of the leading edge.

Some interesting features are also evident in the CTH and DEBRIS3 predictions of the state of the target material. In run 3, the average target material density as predicted by CTH is approximately 12% of ambient. This indicates a significant liquid, if not vaporous, component of the target material in the debris cloud. For run 3, DEBRIS3 predicted that 100% of the shocked and released target material would be liquid and that the density of the shocked and released target material would be approximately 75% of ambient. The near-zero value of the target material density as predicted by CTH in run 4 indicates a material state near complete vaporization for the ejected target material while DEBRIS3 predicted that approximately 24% of the shocked and released target material would be in a vapor state and that 76% would be liquid. The density of the shocked and released target material predicted by DEBRIS3 was 40% of the ambient value indicating a highly expanded material state.

SUMMARY AND CONCLUSIONS

A robust damage assessment methodology for high speed impacts must include the effects of discrete particle impacts as well as the response of the target to impulsive debris cloud loadings. A first principles based scheme has been developed and implemented to determine the amount of material in each of the three states of matter in a debris cloud created by a hypervelocity impact on a thin target. The Tillotson equation-of-state was used to calculate the residual energy in the projectile and target materials upon release from their respective shocked states. Elementary thermodynamic principles were used to determine the percentages of shocked and released projectile and target materials that were melted and/or vaporized during the release process. Using assumed projectile and target geometries, these percentages were then used to calculate the mass of the projectile and target materials in solid, liquid, and gaseous form. Debris cloud velocities were calculated using the principles of momentum and energy conservation; the spread of the debris cloud material was then readily obtained.

The predictions of the debris cloud model were compared against experimental data, the predictions of three different empirically based codes, and against the predictions of one-dimensional and three-dimensional hydrocodes. For single-material projectiles, the predictions of the characterization scheme compared excellently, qualitatively as well as quantitatively, against experimental results, the predictions of a one-dimensional hydrocode, and the predictions of several semiempirical lethality assessment schemes. For multimaterial projectiles, the predictions of the scheme developed herein compared favorably (at least qualitatively) with experimental results and hydrocode predictions. Although some of the quantitative details in the debris cloud model differed from empirical evidence in the case of multimaterial projectiles, it is noted that the debris cloud model presented herein was developed solely through the application of fundamental physical principles without any empirical "adjustment" factors. In this light, the agreement between the elementary theory predictions and the experimental results is encouraging.

The author would like to acknowledge the support of the Air Force Office of Scientific Research Summer Faculty Research Program. In addition, the author is grateful to Mr. Scott Mullin of the Southwest Research Institute and to Ms. Kathy Holian of Los Alamos National Laboratory for their assistance with the implementation of the Tillotson equation-of-state. The assistance of Mr. Danny Brubaker in performing the CTH runs for this study and in analyzing the CTH output is also gratefully acknowledged. Finally, thanks go to Messrs. David Jerome and Ronald Hunt within the Technology Assessment Branch (WL/MNSA) for their guidance and assistance during the course of the research program.

REFERENCES

Bjorkman, M. D., Geiger, J. D., and Wilhelm, E. E., 1987, *Space Station Integrated Wall Design and Penetration Damage Control, Task 3: Theoretical Analysis of Penetration Mechanics*, Boeing Aero-

space Corporation, Final Report, Contract NAS8-36426, Seattle, WA.

Greer, R., and Hatz, M., 1992, *KAPP-II User's Manual, Version 1.1*, Kaman Sciences Corporation, K92-17U(R), Colorado Springs, CO.

Herrmann, W., and Wilbeck, J. S., 1987, "Review of Hypervelocity Impact Penetration Theories," *International Journal of Impact Engineering*, Vol. 5, pp. 307–322.

Jolly, W. H., 1993, "Analytical Prediction of Hole Size Due to Hypervelocity Impact of Spherical Projectiles," Master's Thesis, University of Alabama in Huntsville.

Maiden, C. J., Gehring, J. W., and McMillan, A. R., 1963, "Investigation of Fundamental Mechanism of Damage to Thin Targets by Hypervelocity Projectiles," General Motors Defense Research Laboratory, TR-63-225, Santa Barbara, CA.

Piekutowski, A. J., 1990, "A Simple Dynamic Model for the Formation of Debris Clouds," *International Journal of Impact Engineering*, Vol. 10, pp. 453–471.

Rice, M. H., McQueen, R. G., and Walsh, J. M., "Compression of Solids by Strong Shock Waves," in F. Seitz and D. Turnbull, *Solid State Physics, Vol. 6*, 1958, Academic Press, New York.

Rinehart, J. S., 1975, *Stress Transients in Solids*, HyperDynamics, Santa Fe, NM.

Schonberg, W. P., 1994, "Debris Cloud Material Characterization for Hypervelocity Impacts of Single- and Multi-Material Projectiles on Thin Target Plates," WL-TR-94-7039, Eglin AFB, Florida.

Tillotson, J. H., 1962, "Metallic Equations of State for Hypervelocity Impact," General Dynamics, General Atomic Division, Report No. GA-3216.

Wilbeck, J. S., Scott, P. G., and Lew, T. M., 1988, "Enhanced Fragment Lethality," AFATL-TR-88-105, Eglin AFB, Florida, August.

Yatteau, J. D., Zernow, R. H., and Recht, R. F., 1991a, *Compact Fragment Multiple Plate Penetration Model, Volume I: Model Description*, NSWC-TR-91-399, Dahlgren, Virginia.

Yatteau, J. D., Zernow, R. H., and Recht, R. F., 1991b, *Compact Fragment Multiple Plate Penetration Model, Volume II: Computer Code User's Manual*, NSWC-TR-91-399, Dahlgren, Virginia.